

# Self-Alignment of Plasmonic Gold Nanorods in Reconfigurable Anisotropic Fluids for Tunable Bulk Metamaterial Applications

Qingkun Liu,<sup>†,‡</sup> Yanxia Cui,<sup>‡</sup> Dennis Gardner,<sup>†,§</sup> Xin Li,<sup>‡</sup> Sailing He,<sup>‡,||</sup> and Ivan I. Smalyukh<sup>\*,‡,§,⊥</sup>

<sup>†</sup>Department of Physics, University of Colorado, Boulder, Colorado 80309, <sup>‡</sup>Centre for Optical and Electromagnetic Research, Zhejiang University, Hangzhou 310058, People's Republic of China, <sup>§</sup>Liquid Crystal Materials Research Center, University of Colorado, Boulder, Colorado 80309, <sup>||</sup>Department of Electromagnetic Engineering, Royal Institute of Technology, S-100 44 Stockholm, Sweden, and <sup>⊥</sup>Renewable and Sustainable Energy Institute, University of Colorado, Boulder, Colorado 80309

**ABSTRACT** We demonstrate the bulk self-alignment of dispersed gold nanorods imposed by the intrinsic cylindrical micelle self-assembly in nematic and hexagonal liquid crystalline phases of anisotropic fluids. External magnetic field and shearing allow for alignment and realignment of the liquid crystal matrix with the ensuing long-range orientational order of well-dispersed plasmonic nanorods. This results in a switchable polarization-sensitive plasmon resonance exhibiting stark differences from that of the same nanorods in isotropic fluids. The device-scale bulk nanoparticle alignment may enable optical metamaterial mass production and control of properties arising from combining the switchable nanoscale structure of anisotropic fluids with the surface plasmon resonance properties of the plasmonic nanorods.

**KEYWORDS** Nanorods, liquid crystals, optical metamaterials, self-assembly, plasmonic nanoparticles

Having pre-designed structural units different from those in a conventional matter, metamaterials exhibit many unusual properties of interest from both fundamental science and applications standpoints. However, manufacturing such bulk optical metamaterials with three-dimensional (3D) structure<sup>1–4</sup> using lithography techniques presents a significant challenge, especially for the large-scale production. Mass production of bulk optical metamaterials from self-aligning and self-assembling nanoparticles is poised to revolutionize scientific instruments, technologies, and consumer devices.<sup>5–7</sup> Although the metamaterial self-assembly from nanoparticles remains a significant challenge, recent advances in colloidal science show that it may be realized and the emerging nanoscale alignment and assembly approaches utilize surface monolayers,<sup>8,9</sup> stretched polymer films,<sup>10,11</sup> and functionalized nanoparticles<sup>12,13</sup> but are usually restricted to only short-range ordering, two-dimensional rather than three-dimensional assembly, and limited switching.<sup>7</sup> Tunable metamaterials may potentially be obtained by nanoparticle self-assembly in liquid crystals (LCs)<sup>14</sup> through the LC-mediated realignment and rearrangement of incorporated nanoparticles in response to applied fields. However, experimental realization of such self-assembling switchable metamaterial composites is lacking. In this work, we demonstrate spontaneous long-range orien-

tational ordering of gold nanorods (GNRs) dispersed in surfactant-based lyotropic LCs and use polarizing optical microscopy, darkfield microscopy, spectroscopy, and freeze-fracture transmission electron microscopy (FFTEM) to study these composites on the scales ranging from nanometers to millimeters. We find that the anisotropic fluids in both columnar hexagonal and nematic LC phases impose nematic-like long-range orientational ordering of GNRs with no correlation of their centers of mass but with the GNRs aligning along the LC director  $\mathbf{n}$  (a unit vector describing the average local orientation of cylindrical micelles forming the LC), Figure 1. The unidirectional alignment of nanorods with high order parameter is achieved in bulk samples of thickness ranging from several micrometers to millimeters, over large (approximately square inch) sample areas, and even for nanorods that have length-to-diameter aspect ratios too small to form LC phases in highly concentrated colloidal dispersions. This alignment can be scaled to much smaller and much larger sample volumes and to nanorods with a broad range of length-to-diameter aspect ratios. Furthermore, this nanorod alignment results in a strong polarization sensitivity of surface plasmon resonance (SPR) effects exhibited by the nanostructured composite medium.

GNRs were synthesized using the seed-mediated method (Figure 2a).<sup>15</sup> During the synthesis procedures, we have varied the average length and aspect ratios of GNRs (see Supporting Information) and obtained unidirectional alignment for GNRs of different aspect ratios as described below. We have used anisotropic fluids in nematic and hexagonal

\* Corresponding author, ivan.smalyukh@colorado.edu.

Received for review: 12/20/2009

Published on Web: 03/24/2010



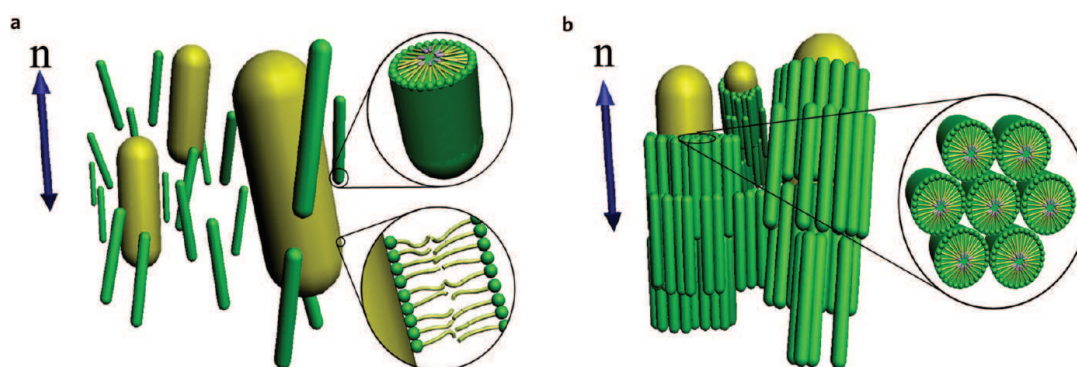


FIGURE 1. Schematic illustration of GNR alignment in the nematic LC. (b) GNR alignment in a columnar hexagonal lyotropic LC phase. The diameter of micelles is 2–3 nm.<sup>16</sup> GNRs have diameter within 15–25 nm and length of ~50 nm.

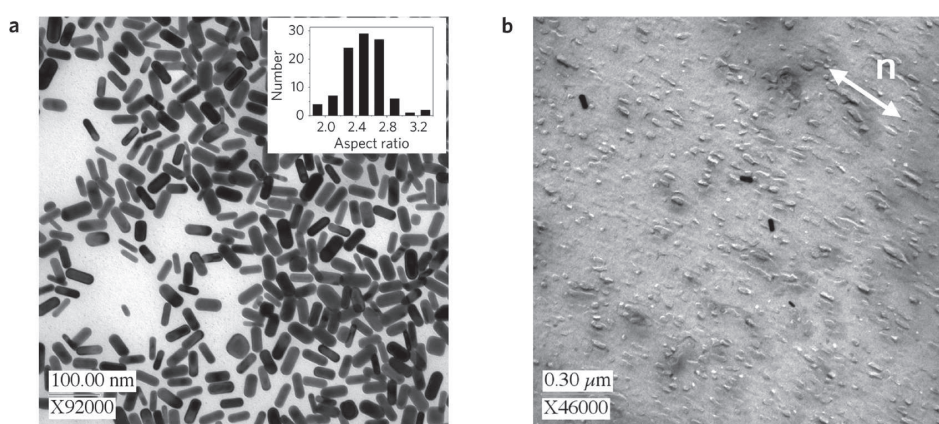
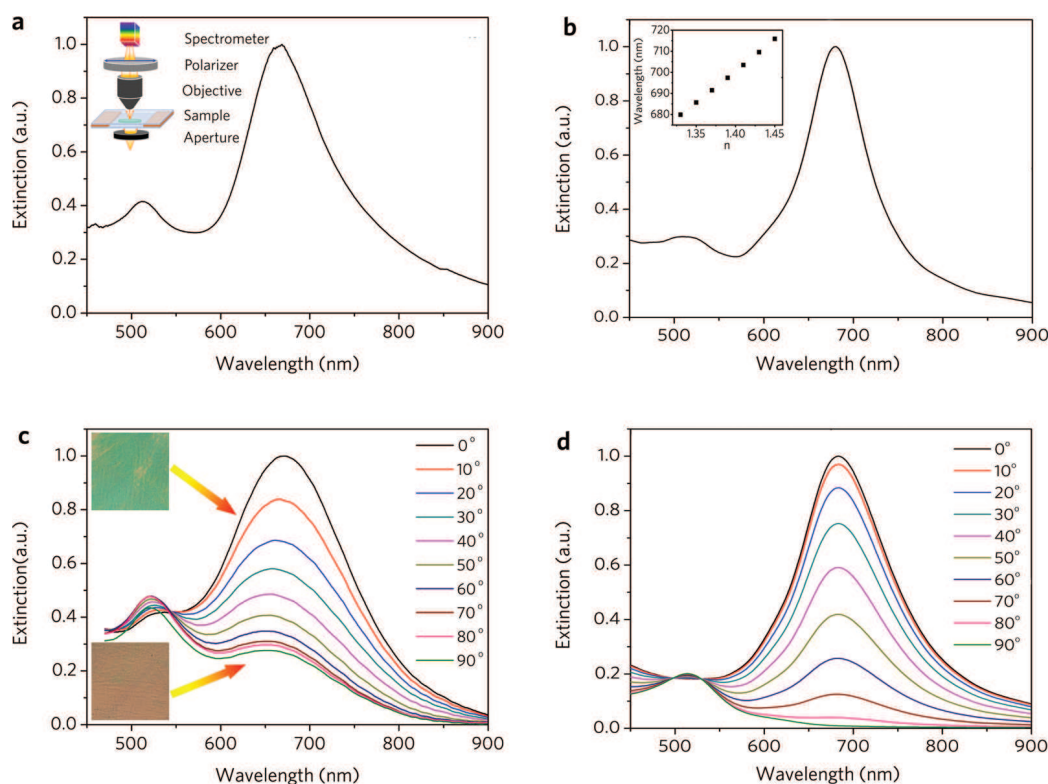


FIGURE 2. (a) TEM micrograph of GNRs. The inset shows the distribution of measured aspect ratios of GNRs which are on average 53 nm long and 21 nm in diameter. (b) FFTEM image revealing the orientation of GNRs in a lyotropic LC matrix evidenced by unidirectional alignment of GNR replicas in the fracture plane.

phases of the CTAB/benzyl alcohol/water ternary system with well-established phase diagram.<sup>16,17</sup> Typically, the LC in the hexagonal phase was prepared using a composition of 25% CTAB, 5% benzyl alcohol (both from Aldrich, used as supplied) and 70% of aqueous suspension of GNRs stabilized by CTAB with GNRs at about  $10^{-8}$  M. This was followed by centrifugation at 3000 rpm for 10 min and ultrasonication for 30 min at room temperature. The samples exhibited no visible aggregates, indicating that GNRs are well-dispersed in the hexagonal H1 phase. The lyotropic LC in the nematic phase was prepared as above but consisted of 25% CTAB and 75% of aqueous GNRs dispersion.<sup>17</sup> The LC phases of studied nanocomposites were further changed by adjusting the surfactant concentration. The hexagonal phase is composed of cylindrical surfactant micelles exhibiting long-range orientational and hexagonal 2D positional ordering while the nematic phase exhibits only long-range orientational ordering.<sup>16,17</sup> Dispersing nanoparticles (especially in anisotropic fluids) is a technical challenge and often requires surfactant stabilization of GNRs.<sup>18,19</sup> The used lyotropic LC is composed of the same surfactant molecules that stabilize GNRs during the synthesis procedures, yielding well-dispersed nanorods in the lyotropic LC host. The LC-GNR composites were sandwiched between two glass plates

separated by 0.01–1 mm gap using Mylar film spacers and uniformly aligned by shearing ( $\mathbf{n}$  on average along the shear direction) or by a strong 11.7 T magnetic field.

The phase behavior, dispersion quality, as well as LC alignment and structures were studied by means of optical microscopy. Polarizing and bright-field optical imaging of GNR-LC composites were performed using an Olympus BX-51 upright polarizing optical microscope with 10 $\times$ , 20 $\times$ , and 50 $\times$  air objectives (all from Olympus) with numerical aperture NA = 0.3–0.9 integrated with the Spot 14.2 Color Mosaic Camera (from Diagnostic Instruments, Inc.). Imaging in the darkfield mode was performed using Eclipse ME600 microscope (from Nikon) equipped with an oil darkfield condenser (NA = 1.43–1.20) and a video camera DXM 1200F (from Nikon); only highly scattered light was collected using a 100 $\times$  air objective (NA = 0.7). The extinction spectra were measured using USB2000 microspectrometers (Ocean Optics) mounted on both optical microscopes. In the optical spectroscopy experiments, the microscope aperture was adjusted and the sample was centered on its stage so that the probing light was always passing through the same circular area of the LC cell while the stage was rotated. The spectra were measured after the unpolarized light passed through the sample and a linear polarizer oriented at a given



**FIGURE 3.** (a) Experimental and (b) computer-simulated extinction spectra of randomly aligned GNRs dispersed in water. The inset of (a) shows the setup used to obtain the SPR spectra. The inset of (b) shows the simulated dependence of SPR peak wavelength as a function of the dispersing medium's refractive index. (c, d) Polarization-sensitive (c) experimental and (d) computer-simulated extinction spectra of GNRs in a columnar phase of the lyotropic LC for different angles between the linear polarizer and the director. The two insets in (c) are transmission optical microscopy images (for a sample area  $0.05 \text{ mm} \times 0.05 \text{ mm}$ ) obtained for unpolarized light passing first through the cell with aligned GNRs and then through a linear polarizer either parallel or perpendicular to the director. A fixed diameter of 21 nm and experimental average nanorod length of 53 nm (based on TEM images, Figure 2a) were used in simulations. The refractive index was set to 1.33 for both water and LC (although it is slightly higher for the LC due to the large concentration of CTAB).

angle with respect to the LC director. Optical imaging and spectroscopy show no evidence of nanoparticle aggregation and both quality and long-term stability of dispersion in LCs are comparable to those in water.

FFTEM images corresponding to different fracture planes (Figure 2b, see the Supporting Information) containing  $\mathbf{n}$  show unidirectional alignment of well-dispersed GNRs along  $\mathbf{n}$  with the rods separated by distances comparable to their length or larger, in stark contrast to the random alignment in isotropic fluids (Figure 2a). Using the FFTEM images similar to those shown in Figure 2b and obtained at different sample depths, we estimate the two-dimensional (2D) orientational order parameter of GNRs in each fracture plane  $S_{2D-\text{fracture}} = 2\langle \cos^2 \theta_{\text{fracture}} \rangle - 1$  by measuring the angles  $\theta_{\text{fracture}}$  between the orientation of long axes of the fracture-plane replicas corresponding to individual rods and their local average orientation  $\mathbf{n}$  in this plane (we use  $>100$  rods for each fracture plane). The 2D order parameter values of GNRs in five different fracture planes are within  $S_{2D-\text{fracture}} = (0.86-0.91)$ , independent of the fracture plane location across the sample, and comparable to order parameter values exhibited by rodlike micelles in calamitic lyotropic LCs.<sup>20</sup>

The optical transmission spectra obtained for random dispersions of GNRs in water show polarization-independent transverse and longitudinal (relative to the nanorod axes) SPR bands at  $\sim 525$  and  $\sim 680$  nm, Figure 3a. In contrast, aligned GNRs in the LC matrix exhibit extinction spectra varying with the angle between the polarizer and GNRs aligned along  $\mathbf{n}$  (Figure 3c). These spectra have been obtained using a microscope with white light passing through a  $4 \text{ mm}^2$  circular aperture, the glass cell with 1 mm gap between glass plates filled with the composite system of GNRs ( $10^{-8} \text{ M}$ ) in the shearing-aligned columnar hexagonal LC and then through a rotatable linear polarizer (inset of Figure 3a). The longitudinal SPR band is the strongest when the polarizer is parallel to  $\mathbf{n}$  and long axes of GNRs but decreases to  $\sim 27\%$  of its initial value when the polarizer is perpendicular to  $\mathbf{n}$ . In contrast, the transverse SPR peak is the strongest when the polarizer is orthogonal to  $\mathbf{n}$  but becomes partially suppressed when rotating the polarizer toward  $\mathbf{n}$ . The polarization sensitivity of the transverse SPR band is less pronounced than that of the longitudinal one. The SPR peaks of GNRs in LCs are slightly shifted to longer wavelengths as compared to the isotropic dispersions of the same nanorods (Figure 3). This is a result of the increase of

the solvent's refractive index from that of water 1.33 to  $\sim 1.4$  as more and more CTAB is added to form nematic or columnar hexagonal phases (in agreement with computer simulations shown in the inset of Figure 3b). The longitudinal SPR band of GNRs in the LC is polarized (Figure 3c,d and Figure S1a in Supporting Information) and its peak slightly shifts when changing the angle between  $\mathbf{n}$  and polarizer (Figure 3c and Figures S1 and S2 in Supporting Information). Using the experimental spectra, one can estimate the three-dimensional order parameter of GNRs in the uniaxial LC matrix defined as  $S_{3D} = (3\langle \cos^2 \theta_{3D} \rangle - 1)/2$ , where  $\theta_{3D}$  is an angle between  $\mathbf{n}$  and GNRs. The order parameter of GNRs can be deduced from the polarized optical transmission data by determining the absorbance  $A$  for polarizer orientations parallel and perpendicular to  $\mathbf{n}$  and using expression

$$S_{3D} = \frac{A_{\parallel} - A_{\perp}}{A_{\parallel} + 2A_{\perp}}$$

Within the studied  $4 \text{ mm}^2$  area of 1 mm thick shearing-aligned columnar hexagonal LC sample, the large-scale alignment of  $\mathbf{n}$  is imperfect and micrometer-sized domains with slightly misaligned  $\mathbf{n}$  are visible. This feature is typical of shearing-aligned columnar LCs and results in apparent lowering of the 3D order parameter  $S_{3D} \approx 0.46$ , although the local values of order parameter (as will be shown below using local characterization in darkfield mode) are much higher and consistent with the FFTEM data.

We have simulated the extinction spectra using the finite-difference time-domain (FDTD) method<sup>21</sup> and wavelength-dependent properties of gold obtained from ref 22 (Figure 3b,d). For LC dispersions, we have assumed perfect alignment of GNRs along  $\mathbf{n}$  ( $S_{3D} = 1$ ) with their centers of mass arranged periodically at 80 nm distances comparable to an average interparticle spacing in experiments, Figure 2b. The longitudinal SPR peak is selectively excited for linear polarization parallel to  $\mathbf{n}$  and only the transverse mode is excited for light polarized perpendicular to  $\mathbf{n}$ ; both modes exist at intermediate linear polarization directions. Simulated and experimental results show qualitative resemblance (Figure 3), although the experimental extinction spectra display incompletely suppressed partial excitation of the transverse and longitudinal SPR modes at, respectively, parallel and orthogonal orientations of the polarizer with respect to  $\mathbf{n}$ . This is an expected result since  $S_{3D} < 1$  in the studied samples (Figure 2b), the large-scale alignment on the millimeter scales of the sample probed by spectroscopy is imperfect, and the birefringent LC medium affects polarization of the used probing light as it traverses the millimeter-thick sample (Figures S1 and S2 in Supporting Information). Influence of these factors is partially mitigated in thinner samples. The experimental spectral bands are slightly broader than the computer-simulated ones (Figure 3); this is a result of the relatively broad distribution of nanorod aspect ratios (inset of Figure 2a), as demonstrated in Figure S1 (Supporting Information).

Nematic lyotropic LC can be realigned by applying fields, similar to that in displays and spatial light modulators.<sup>16,17</sup> The GNR-LC composites have a potential for tuning SPR properties using external fields. In order to test this hypothesis, the nematic LC with GNRs at about  $10^{-8}$  M was filled into a 0.3 mm thick and 3 mm wide rectangular capillary (sealed at the ends using epoxy) and then put into a 11.7 T magnetic field. In a sample annealed from isotropic phase, rodlike micelles and  $\mathbf{n}$  orient along the magnetic field and preserve this uniform alignment after the field is turned off (Figure 4). When the rectangular capillary sample with aligned  $\mathbf{n}$  along the capillary length is rotated between crossed polarizers, it behaves as a uniaxial crystal plate, showing extinction at orientations with  $\mathbf{n}$  parallel to a polarizer or an analyzer (Figure 4d) and orientation-dependent transmitted light intensity for the intermediate angles (Figure 4c). Polarized SPR spectra taken for samples with magnetically realigned  $\mathbf{n}$  show that the LC matrix aligns GNRs along  $\mathbf{n}$  (Figure 4a) and GNR orientation in the nematic fluid can be controlled by magnetic fields via switching of  $\mathbf{n}$ . Furthermore, experimental SPR spectra (Figure 4a) are in a good agreement with the simulations (Figure 4b) and qualitatively resemble those obtained for GNRs in a columnar hexagonal LC host (Figure 3). The longitudinal and transverse SPR peaks are nearly completely suppressed for polarizations orthogonal and parallel to  $\mathbf{n}$ , respectively (Figure 4a), indicating a much better large-scale magnetic field alignment of the LC matrix as compared to shear-induced alignment of hexagonal-phase samples. The estimated value of 3D order parameter of GNRs  $S_{3D} \approx 0.86$  is higher than that in the shear-aligned columnar hexagonal LC samples. By repeating these experiments for two different light transmission optical paths of the rectangular capillary (0.3 mm and 3 mm), we obtain the same value of  $S_{3D} \approx 0.86$ , implying uniform bulk alignment of GNRs across the sample. Although the elastic alignment of GNRs along  $\mathbf{n}$  occurs spontaneously, the direction of  $\mathbf{n}$  and ensuing orientation of GNRs can be prechosen and switched using magnetic fields.

GNR alignment along  $\mathbf{n}$  is mediated by the LC elasticity and tangential surface anchoring at the interfaces of nanorods and LC.<sup>23,24</sup> For the nematic LC, assuming that the Frank elastic constants for splay, twist, and bend are equal to their average value  $K$ , the elastic energy cost of rod realignment<sup>23</sup> to an angle  $\theta$  from its equilibrium  $\theta = 0$  orientation can be estimated as  $\Delta F_{\text{elastic}} \approx 2\pi K \theta^2 L / \ln[2L/R]$  (note that the rods studied here have rather small aspect ratios and only rough estimates are possible by using this equation). Taking  $K \approx 1 \text{ pN}$  (typical for lyotropic nematics) and dimensions of GNRs, one finds  $\Delta F_{\text{elastic}} \approx 3 \times 10^{-19} \theta^2 J$  larger than the thermal energy  $K_B T$  unless  $\theta$  is very small.<sup>24</sup> Therefore, GNR reorientations away from  $\mathbf{n}$  are hindered by the medium's elasticity, resulting in the observed alignment. GNR-induced elastic distortions in the surrounding LC matrix also lead to elasticity-mediated interaction forces that can

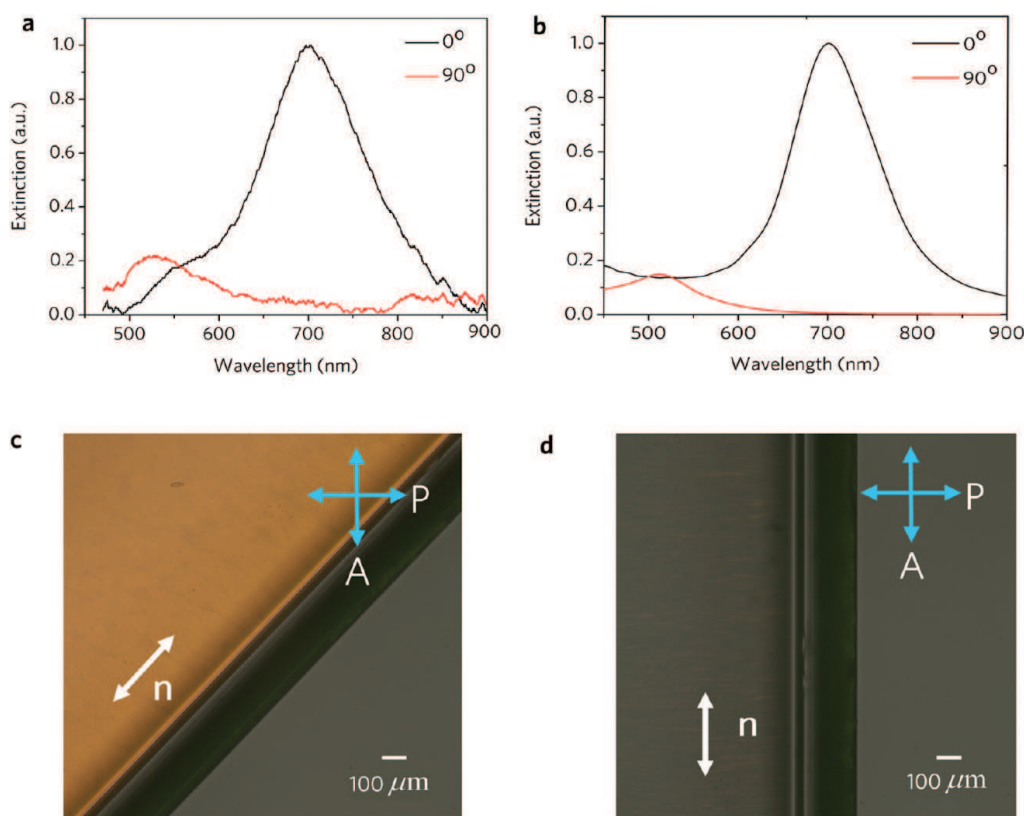


**FIGURE 4.** (a) Experimental and (b) simulated extinction spectra of GNRs in a nematic LC realigned by a magnetic field. (c, d) Polarizing optical microscopy textures of GNR-doped LC for two different orientations of the director between crossed polarizers (blue double arrows) showing high-quality long-range alignment (the area of the image is 1 mm × 1 mm). The simulation was carried out for the diameter of GNRs fixed to 17 and 50 nm average length obtained from experimental TEM images.

be both attractive and repulsive, depending on the orientation of the interparticle separation vector with respect to  $\mathbf{n}$ . Since the size of nanorods is smaller than the surface anchoring extrapolation length  $K/W \sim 10^{-7}m$ , the maximum elasticity- and surface anchoring-mediated binding energy for GNRs aligned along  $\mathbf{n}$  can be estimated as  $2WR^2 \leq K_b T$  and is comparable to or smaller than the thermal energy, where  $W \sim 10^{-5}J/m^2$  is the typical surface anchoring strength at the solid–LC interface.<sup>25</sup> The above estimates show that the elasticity-mediated interactions of GNRs with the surrounding nematic matrix are strong enough to induce uniform long-range alignment of rods but the ensuing interparticle interactions are weak and comparable in strength to thermal energy, so that they are not causing aggregation. This explains why the long-term stability of the studied GNR dispersion in nematic LCs is comparable to that in water at similar concentrations: the CTAB surfactant layer effectively stabilizes GNRs against aggregation due to the van der Waals and other interparticle forces present in both LC and water while the weak elasticity-mediated anisotropic forces (present only in the LC hosts) are comparable in strength to thermal fluctuations and do not cause colloidal aggregation. In columnar hexagonal LC, the colloidal stability is further enhanced by the two-dimensional solid-like structure in the plane orthogonal to columns (limiting motion of GNRs in this plane). At the same time, in both water-based and LC-based

highly concentrated dispersions with interparticle distances comparable to particle diameters, the dispersions are usually stable only for several days; further improvement of long-term stability of these highly concentrated dispersions (including that in the presence of applied magnetic and electric fields) is of critical importance from the standpoint of self-assembly-based metamaterial fabrication.

Since the Onsager critical concentration for nematic ordering is  $\varphi \sim 8R/L$ ,<sup>24</sup> the used GNRs with relatively large radius to length aspect ratios  $R/L = 0.2–0.4$  are not expected to order spontaneously when dispersed in isotropic solvents even at high concentrations. In the LC anisotropic fluids, however, the nanorod alignment is induced by elasticity even at very dilute GNR concentrations. This is demonstrated in Figure 5 showing aligned individual nanorods separated by distances 10–30 μm (~3 orders of magnitude larger than the nanoparticle dimensions). The scattering light intensity from aligned GNRs is the strongest when incident light polarization is parallel to  $\mathbf{n}$  and minimum for the polarizer orthogonal to  $\mathbf{n}$ , Figure 5. Since the rods are undergoing Brownian motion while remaining aligned and the signal integration times are long (0.25 s), the scattering spectra in Figure 5d are obtained by averaging signals over the individual rods within the field of view, assuring that the same GNRs are present within the field of view during the duration of the experiment. The estimated order parameter

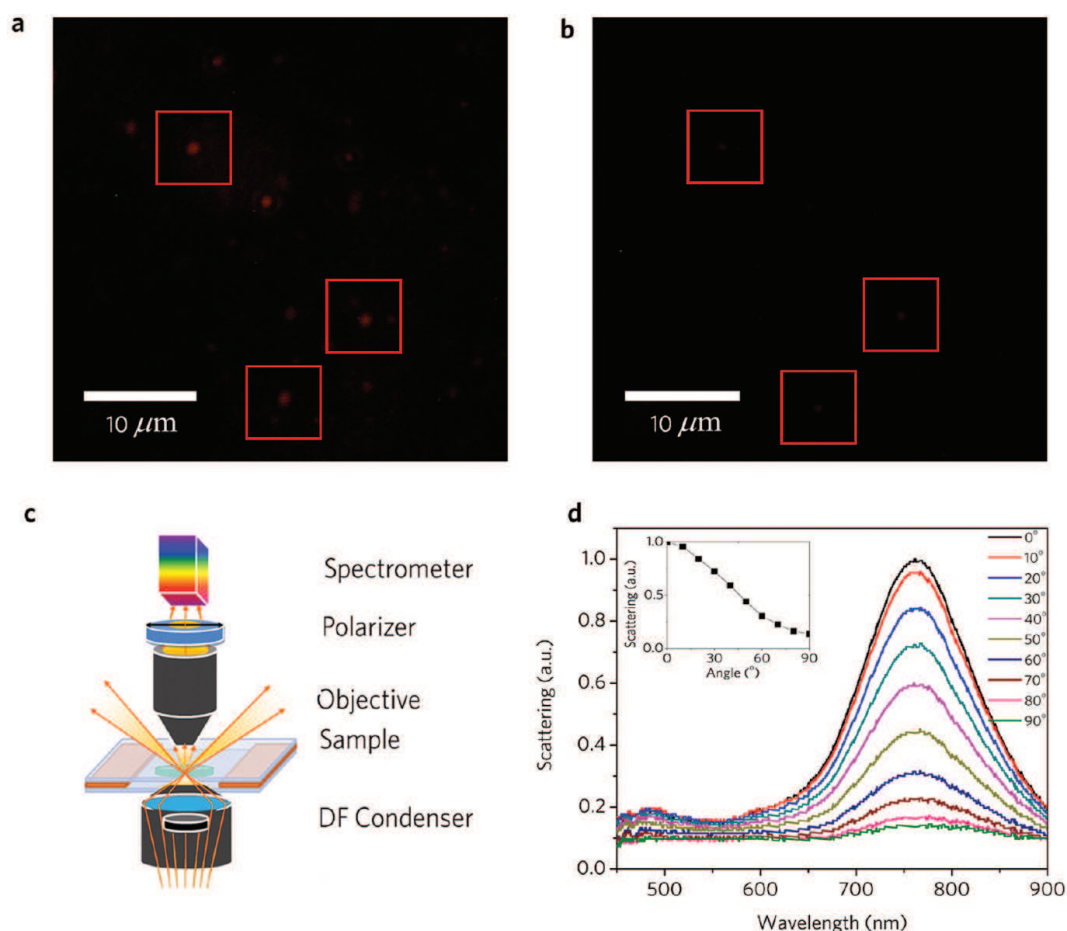


FIGURE 5. (a, b) The darkfield scattering images of individual aligned GNRs at about  $10^{-9}$  M concentration in the columnar hexagonal LC obtained for polarizations (a) parallel and (b) perpendicular to the director. (c) Schematics of the used setup for darkfield scattered light imaging and spectroscopy. (d) Scattering intensity as a function of wavelength for signal integration time of 0.25 s and for different linear polarizations of incident light varying from parallel to perpendicular to the director and GNRs; the longitudinal SPR peak for used GNRs is at  $\sim 760$  nm. The inset of (d) shows scattering intensity as a function of the angle between a polarizer and the director in the aligned LC. The shearing-aligned columnar hexagonal LC with  $10^{-9}$  M concentration of GNRs is studied in a  $6 \mu\text{m}$  thick cell. The used GNRs are on average 68 nm long and 20 nm in diameter.

based on these data is rather high ( $S_{3D} \approx 0.88$ ), and its value is consistent with the 2D order parameter measured in the columnar hexagonal LC using FFTEM images in different fracture planes for slightly shorter GNRs (Figure 2). Polarized light scattering of individual GNRs resolved by imaging the scattered light in a darkfield mode reveals that all rods within the field of view orient along  $\mathbf{n}$  (Figure 5) and such alignment is, in principle, achievable on the scales of meters and larger.

In conclusion, we have demonstrated aggregation-free elastic self-alignment of nanorods dispersed in LCs and their realignment by shearing and magnetic fields. The unidirectional self-ordering of gold nanorods with high 3D order parameter values approaching 0.9 gives rise to the strong polarization sensitivity of surface plasmon resonance effects, showing the potential for LC-mediated oriented self-assembly of bulk optical metamaterials with tunable and switchable properties. Our method of device-scale large-volume bulk alignment of nanorods extends the capabilities provided by other alignment methods<sup>8–13,23,24,26–29</sup> and can be used for a broad range of rodlike particles with different

length-to-diameter aspect ratios and chemical compositions. Furthermore, the observed strong orientation dependence of SPR spectra may allow for novel orientation sensors<sup>30</sup> and plasmonic versions of 3D label-free imaging of director structures in liquid crystals.<sup>31</sup>

**Acknowledgment.** This work was supported by the International Institute for Complex Adaptive Matter (ICAM-I2CAM), Renewable and Sustainable Energy Initiative and Innovation Initiative Seed Grant Programs of University of Colorado, the NSF grants DMR 0645461, DMR-0820579, and DMR-0847782, and the National Basic Research program of China (2004CB719800). We thank Corinne Beier, Noel Clark, Jun Qian, Julian Evans, Tom Lubensky, Won Park, Leo Radzihovsky, Richard Shoemaker, and Qiuqiang Zhan for discussions.

**Supporting Information Available.** Details of nanoparticle synthesis, sample preparation, characterization techniques and computer simulations. This material is available free of charge via the Internet at <http://pubs.acs.org>.

## REFERENCES AND NOTES

- (1) Yao, J.; Liu, Z.; Liu, Y.; Wang, Y.; Sun, C.; Bartal, G.; Stacy, A. M.; Zhang, X. *Science* **2008**, *321*, 930.
- (2) Valentine, J.; Zhang, S.; Zentgraf, T.; Ulin-Avila, E.; Genov, D. A.; Bartal, G.; Zhang, X. *Nature* **2008**, *455*, 376.
- (3) Shalaev, V. M. *Nat. Photonics* **2007**, *1*, 41.
- (4) Soukoulis, C. M.; Linden, S.; Wegener, M. *Science* **2007**, *315*, 47.
- (5) Liu, N.; Liu, H.; Zhu, S.; Giessen, H. *Nat. Photonics* **2009**, *3*, 157.
- (6) Alu, A.; Engheta, N. *Nat. Photonics* **2008**, *2*, 307.
- (7) Stebe, K. J.; Lewandowski, E.; Ghosh, M. *Science* **2009**, *325*, 159; Lapointe, C. P.; Mason, T. G.; Smalyukh, I. I. *Science* **2009**, *326*, 1083.
- (8) Swami, A.; Selvakannan, P. R.; Pasricha, R.; Sastry, M. *J. Phys. Chem. B* **2004**, *108*, 19269.
- (9) Fukuto, M.; Heilmann, R. K.; Pershan, P. S.; Badia, A.; Lennox, R. B. *J. Chem. Phys.* **2004**, *120*, 3446.
- (10) Shenhar, R.; Norsten, T. B.; Rotello, V. M. *Adv. Mater.* **2005**, *17*, 657.
- (11) Perez-Juste, J.; Rodrigues-Gonzalez, B.; Mulvaney, P.; Liz-Marzan, L. *Adv. Funct. Mater.* **2005**, *15*, 1065–1071.
- (12) Elghanian, R.; Storhoff, J. J.; Mucic, R. C.; Letsinger, R. L.; Mirkin, C. A. *Science* **1997**, *277*, 1078.
- (13) Hegmann, T.; Qi, H.; Marx, V. M. *J. Inorg. Organomet. Polym. Mater.* **2007**, *17*, 483.
- (14) Khoo, I. C.; Werner, D. H.; Liang, X.; Diaz, A. *Opt. Lett.* **2006**, *31*, 2592.
- (15) Perez-Juste, J.; Liz-Marzan, L. M.; Carnie, S.; Chan, D. Y. C.; Mulvaney, P. *Adv. Funct. Mater.* **2004**, *14*, 571.
- (16) Montalvo, G.; Valiente, M.; Todenas, E. *J. Colloid Interface Sci.* **1995**, *172*, 494.
- (17) Clawson, J. S.; Holland, G. P.; Alam, T. M. *Phys. Chem. Chem. Phys.* **2006**, *8*, 2635.
- (18) Kumar, P. S.; Pal, S. K.; Kumar, S.; Lakshminarayanan, V. *Langmuir* **2007**, *23*, 3445.
- (19) Zhang, S.; Leem, G.; Srisombat, L.; Lee, T. R. *J. Am. Chem. Soc.* **2008**, *130*, 113.
- (20) Halle, B.; Quist, P.-O.; Furó, I. *Phys. Rev. A* **1992**, *45*, 3763.
- (21) Tavlove, A. *Computational Electrodynamics: The Finite-Difference Time-Domain Method*; Artech House: Norwood, 1995.
- (22) Palik, E. D. *Handbook of Optical Constants of Solids*; Academic Press: New York, 1998.
- (23) Brochard, F.; de Gennes, P.-G. *J. Phys. (Paris)* **1970**, *31*, 691. Rault, J.; Cladis, P. E.; Burger, J. P. *Phys. Lett.* **1970**, *32 A*, 199–200. Chen, S.-H.; Amer, N. M. *Phys. Rev. Lett.* **1983**, *51*, 2298–2301. Lapointe, C.; Hultgren, A.; Silevitch, D. M.; Felton, E. J.; Reich, D. H.; Leheny, R. L. *Science* **2004**, *303*, 652. Smith, C. J.; Denniston, C. J. *Appl. Phys.* **2007**, *101*, 014305.
- (24) Smalyukh, I. I.; Butler, J.; Shrout, J. D.; Parsek, M. R.; Wong, G. C. L. *Phys. Rev. E* **2008**, *78*, 030701(R).
- (25) Smalyukh, I. I.; Lavrentovich, O. D.; Kuzmin, A. N.; Kachynskii, A. V.; Prasad, P. N. *Phys. Rev. Lett.* **2005**, *95*, 157801.
- (26) Baker, J. L.; Widmer-Cooper, A.; Toney, M. F.; Geissler, P. L.; Alivisatos, A. P. *Nano Lett.* **2010**, *10*, 195–201.
- (27) Lynch, M. D.; Patrick, D. L. *Nano Lett.* **2002**, *2*, 1197–1201.
- (28) Ahmed, W.; Kooij, E. S.; van Silfhout, A.; Poelsema, B. *Nano Lett.* **2009**, *9*, 3786–3794.
- (29) Wu, K.-J.; Chu, K.-C.; Chao, C.-Y.; Chen, Y.-F.; Lai, C.-W.; Kang, C.-C.; Chen, C.-Y.; Chou, P.-T. *Nano Lett.* **2007**, *7*, 1908–1913.
- (30) Sonnichsen, C.; Alivisatos, A. P. *Nano Lett.* **2005**, *5*, 301–304.
- (31) Kachynski, A. V.; Kuzmin, A. N.; Prasad, P. N.; Smalyukh, I. I. *Appl. Phys. Lett.* **2007**, *91*, 151905.

# SUPPORTING INFORMATION:

## Self-Alignment of Plasmonic Gold Nanorods in Reconfigurable Anisotropic Fluids for Tunable Bulk Metamaterial Applications

*Qingkun Liu,<sup>1,2</sup> Yanxia Cui,<sup>2</sup> Dennis Gardner,<sup>1,3</sup> Xin Li,<sup>2</sup> Sailing He,<sup>2,4</sup> Ivan I.*

*Smalyukh<sup>1,3,5\*</sup>*

<sup>1</sup>Department of Physics, University of Colorado, Boulder, Colorado 80309, USA

<sup>2</sup>Centre for Optical and Electromagnetic Research, Zhejiang University, Hangzhou  
310058, People's Republic of China

<sup>3</sup>Liquid Crystal Materials Research Center, University of Colorado, Boulder, Colorado  
80309, USA

<sup>4</sup>Department of Electromagnetic Engineering, Royal Institute of Technology, S-100 44  
Stockholm, Sweden

<sup>5</sup>Renewable and Sustainable Energy Institute, University of Colorado, Boulder, Colorado  
80309, USA

\* Corresponding author E-mail: [smalyukh@colorado.edu](mailto:smalyukh@colorado.edu)

## **1. Synthesis of gold nanorods.**

To synthesize GNRs, we have used the seed-mediated method. Typically 0.1mL of an aqueous 0.025M solution of  $\text{HAuCl}_4 \cdot 3\text{H}_2\text{O}$  was added to 10mL of a 0.10M CTAB solution in a conical flask. The solution appeared bright brown-yellow in color when it was gently mixed by stirring. Then 0.6mL of an aqueous 0.01M ice-cold  $\text{NaBH}_4$  solution was added, followed by vigorous stirring for 2 min. The seed solution was used within 40 min. Then 5 mL deionized water, 5 mL of 0.20M CTAB, 0.200mL of 0.025M  $\text{HAuCl}_4 \cdot 3\text{H}_2\text{O}$ , and 0.040mL of 0.016M  $\text{AgNO}_3$  solutions were added to a conical flask, followed by gentle mixing. The solution, then, appeared bright brown-yellow in color as well. Then 0.090mL of 0.08M ascorbic acid was added to it. The solution became colorless after adding and mixing ascorbic acid. Finally, 0.012 mL of seed solution was added, and left undisturbed at  $27^\circ\text{C}$  for at least 10 hours. Then the sample was centrifuged at 3000 rpm for 30 min and re-dispersed in deionized water to make the concentration of GNRs ten times higher than in the former solution. The TEM image of obtained GNRs is shown in Figure 2a. In our studies, the GNR diameter was varied within 15-22nm and the length-to-diameter aspect ratio was varied within 2.1-3.4.

## **2. Freeze-fracture TEM imaging.**

The nano-scale structures in GNR-LC composites were visualized using FFTEM. A small quantity ( $\sim 2\text{-}4\mu\text{l}$ ) of GNR-LC mixture was deposited on a copper disc forming a droplet that was rapidly quenched in liquid propane to the temperature  $< -183^\circ\text{C}$ . The sample was then fractured by slicing off the top of the droplet with a knife in a cold vacuum  $-140^\circ\text{C}$  at  $\sim 10^{-6}$  mbar. The fractured surface was shadowed with 2nm of a

platinum-carbon alloy at  $45^\circ$  for image contrast and  $\sim 30\text{nm}$  of carbon normal to the fractured plane to improve mechanical stability. The copper disc with the shadowed sample is then removed from vacuum, warmed to room temperature, washed in de-ionized water, ethanol, and ethyl acetate to remove the LC host and GNRs leaving behind the Pt-C replicas of the fracture plane. The Pt-C replicas are imaged using TEM revealing the topographic structure at the fractured plane, as shown in Figure 2b. In our experiment several GNRs did not completely wash off and appear as dark rods in the image. The replicas show unidirectional alignment of GNRs along the LC director  $\mathbf{n}$ , Figure 2b. The electron microscopy images in Figure 2b suggest that the rods in the LC are well-dispersed, separated by distances comparable to their length or larger, and aligned.

### 3. Computer simulations of SPR spectra

The 3D finite-difference time-domain (FDTD) method<sup>S1</sup> was used to simulate optical properties of GNR-LC composites (Figures 3b,d and 4b). The method solves Maxwell's equations by first discretizing the equations via central differences in time and space and then numerically solving these equations in software. For simplicity, we have assumed that the GNRs in the LC are perfectly aligned and spaced periodically with the fixed lattice period. The spectra in Figures 3b,d and 4b were calculated for rods of average length and aspect ratios. The extinction spectra shown in Figure S1 were calculated using an experimental distribution function of GNR aspect ratios (Figure 2a) and superposition of results to obtain the response by utilizing the 3D Rigorous Coupled Mode Analysis (RCWA) method.<sup>S2</sup> The methods represent 3D periodic structures with spatial refractive index distribution in the studied medium consisting of both dielectric

(liquid crystal) and dispersive lossy materials (GNRs). The results are obtained for the incident plane waves with different linear polarizations. Figure S1 shows that the experimental bands in Figures 3 and 4 are broader than the respective computer simulated data on the same figures predominantly due to the polydispersity of nanorod sizes.

#### **4. Polarization dependence of SPR spectra**

The magnitude of the longitudinal SPR band of GNRs in the LC is polarization dependent (Fig. S2a) and its resonant peak exhibits a noticeable shift when the angle between  $\mathbf{n}$  and the linear polarizer changes upon sample rotation (Fig. S2b). These dependencies result from a combination of the following effects: (1) dependence of the SPR magnitude on the rod orientation; (2) orientational order parameter  $S \leq 0.9$  exhibited by GNRs; (3) complex light propagation in an anisotropic LC with splitting into the ordinary and extraordinary waves and polarization state changing as the light traverses the anisotropic medium; (4) polarization-sensitive effective refractive index of the LC surrounding GNRs; (5) partial depolarization of light after passing objective and condenser lenses when the spectra are obtained using a spectrometer mounted on a microscope. In the thick bulk samples of thickness  $d \sim 1\text{mm}$ , these effects are especially strongly pronounced as  $\Delta n \cdot d \gg \lambda$  (Figure S1), despite of the rather small optical anisotropy of the used lyotropic LC ( $\Delta n \sim 0.01$ ). To demonstrate that the anisotropic nature of the surrounding LC matrix can significantly influence the SPR spectra and make them different from that of aligned nanorods in isotropic media, we compare computer simulated angular dependencies of amplitude and wavelength of the longitudinal SPR peak with the experimental data, Figure S2. The anisotropic nature of

the medium and issues 2-4 above result in angular dependence of SPR peak wavelength, Figure S2b (not expected for perfectly-aligned nanorods in isotropic media) and modify angular dependence of the SPR peak magnitude, Figure S2b. It is therefore natural that the best agreement between computer simulated results for isotropic media and experimental results for anisotropic fluids is obtained for the polarizer orientation parallel to  $\mathbf{n}$  (Figure S2). The polarization sensitivity of the SPR peak wavelength (Figure S2b) can be used to obtain metamaterials with tunable properties, especially if LCs with high values of optical anisotropy (such as  $\sim 0.2$ , typical for the thermotropic LC materials) are used.

The polarized SPR spectra and the estimated values of order parameter  $S_{3D}$  are also influenced by the microscope optics which causes partial depolarization of light used to obtain these spectra. For example, Figure S3 is obtained in a darkfield geometry similar to that of Figure 5 except that the linear polarizer was placed between the light source and the darkfield condenser. This figure demonstrates that the polarized light scattering spectra are affected by the partial depolarization of light by high-numerical-aperture condenser and scattering geometry; this partial depolarization results in lowering of the estimated 3D order parameter values ( $S_{3D} = 0.71$  vs.  $S_{3D} = 0.88$  for the data on Figure 5d obtained in the darkfield experiment where the effects of light depolarization are partially mitigated). The used objectives cause partial depolarization of light too, although less significant. Therefore, the actual values of order parameter of GNRs in the lyotropic LCs might be slightly higher than those estimated using Figures 3-5.

## SUPPLEMENTARY REFERENCES

S1. Tavlove, A. Computational Electrodynamics: The Finite-Difference Time-Domain Method, *Artech House*, Norwood, 1995.

S2. Moharam, M. G. & Gaylord, T. K. *J. Opt. Soc. Am. A* **1986**, 3, 1780.

## SUPPLEMENTARY

## FIGURES

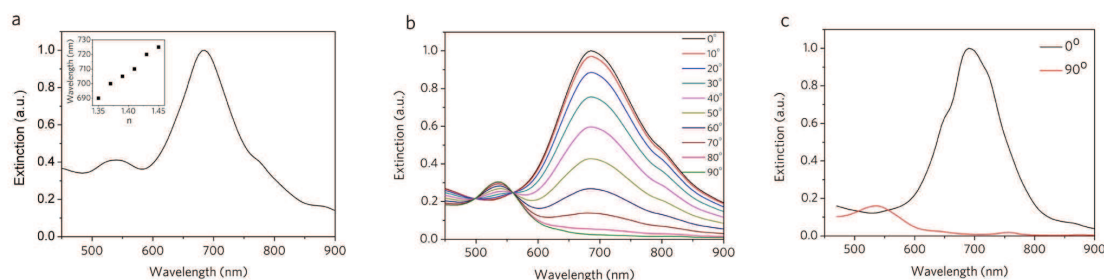


**Figure S1.** Computer-simulated spectra obtained using the RCWA method<sup>S2</sup> with the spectra on (a), (b), and (c) corresponding to FDTD-simulated spectra in Figures 3b, 3d, and 4b, respectively. Compared to the spectra obtained using the FDTD method, the RCWA-calculated spectra have broader bands and display small bumps/shoulders, which stem from solving the full vectorial Maxwell's equations in the Fourier domain and accounting for nanorod size polydispersity using the distributions similar to the one shown in the inset of Figure 2a.

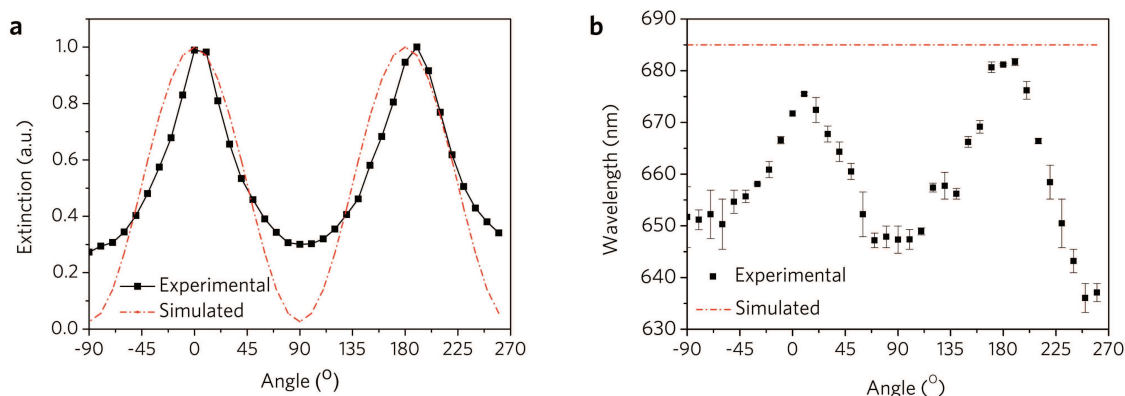


**Figure S2.** The experimental and simulated dependences of (a) amplitude and (b) wavelength shift of the longitudinal SPR peak varying with changing the angle between the polarizer and  $\mathbf{n}$ .

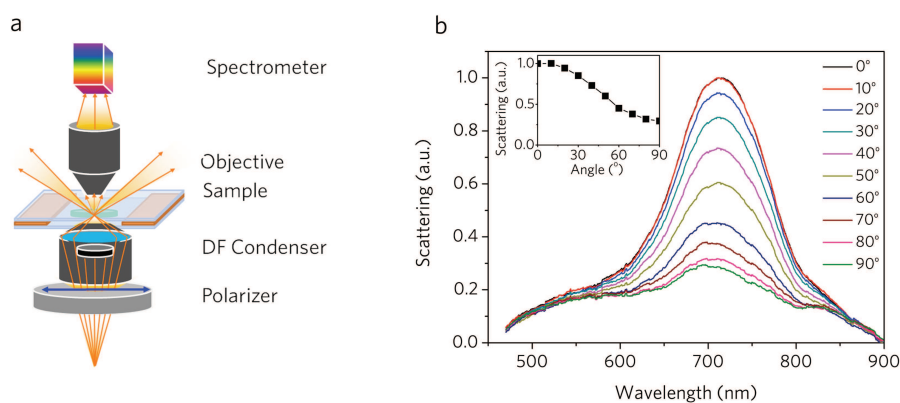


**Figure S3.** (a) A configuration of polarized darkfield microscopy with a polarizer placed between the lightsource and the darkfield condenser. (b) Scattering intensity as a function of wavelength for different linear polarizations of incident light varying from parallel to perpendicular to  $\mathbf{n}$  and GNRs. The inset of (b) shows scattering intensity as a function of the angle between a polarizer and  $\mathbf{n}$  in the aligned LC. The used GNRs are on average 68nm long and 20nm in diameter.